JARTE
Journal of Applied Research in Technology & Engineering

5(2): 53-62, 2024
https://doi.org/10.4995/jarte.2024.20655
Received: November 7, 2023; Accepted: January 13, 2024; Published: July 31, 2024

CFD-BASED INVESTIGATION OF TURBULENT FLOW BEHAVIOR IN 90-DEG PIPE BENDS

Rilwan Kayode Apalowo [a,b,*], Cletus John Akisin [c]

[a] School of Mechanical Engineering, Universiti Sains Malaysia, 14300, Nibong Tebal, Malaysia.
[b] Department of Mechanical Engineering, Federal University of Technology, Akure, 340252, Akure, Nigeria.
[c] Department of Mechanical, Materials and Manufacturing Engineering, University of Nottingham, NG7 2RD, Nottingham, United Kingdom.

[a] rkapalowo@usm.my, [c] rkapalowo@futa.edu.ng

Abstract:

This work investigated the influence of bend curvature on turbulent flow parameters through a 90° pipe bend using the numerical CFD method implemented in ANSYS Fluent. The numerical predictions were validated to be in good agreement with existing experimental measurements. The turbulence of the secondary motion was found to be generally stronger at the outer end of the pipe bend, with the most adverse effect recorded at about 45° along the bend. It was also observed that the RMS velocity is larger near the wall, especially at the outer wall region, and it is highest at 45° due to an increase in the circulation of dean vortices, indicating a turbulence generation. In addition, the RMS velocity increases downstream due to an additional mean strain resulting from secondary flow formation as the flow travels through the bend. Furthermore, larger static pressure and turbulent viscosity were observed at the outer wall due to the flow deceleration and swirling. Therefore, it can be established that the bend curvature affects the stability of the flow field inside a pipe bend.

Keywords: CFD analysis; pipe bend; flow velocity; turbulent viscosity; static pressure.

Cite as: Apalowo, R.K., Akisin, C.J. (2024). CFD-based investigation of turbulent flow behavior in 90-deg pipe bends. *J Appl Res Eng Technol & Engineering, 5*(2), 53-62. https://doi.org/10.4995/jarte.2024.20655

1. Introduction

Understanding curved pipes' turbulent flow mechanism is vital in the design of various engineering applications, such as exhaust gas manifolds, heat exchangers, process equipment, and nuclear reactors. In these applications, turbulent flow through the pipes frequently gives rise to pressure drop and secondary motion and sometimes generates low-frequency vibration. The behavior of the secondary motion of turbulent flow and the sensitivity of turbulence and pressure drop to different bends has been a topic of great research interest. Flow parameters are significant in curved pipes' thermofluid dynamic designs with circular cross-sections. Computation of the turbulence flow parameters for single-phase turbulent flow around the curvature path of a curved pipe will not only aid the understanding of the behavior of the flow around the bend but also enhance the dynamic design.

In general, the investigation of turbulent flow in curved pipe channels has been conducted using different techniques, including numerical modeling and simulation, theoretical analysis, and experimental measurements. Theoretical and numerical models have been developed to model turbulent flow in curved pipes, and implemented to solve these models numerically (Apalowo, 2022). Boersma and Nieuwstadt (1996) developed a large eddy simulation (LES) model to compute the mean velocity of a fully developed turbulent flow in a pipe bend. They established the bend curvature's effect on the flow's mean velocity profile. Spedding et al. (2004) proposed empirical methods for computing the pressure drop of turbulent flow in elbow pipe bends. Schiestel (2010) developed a statistical model for turbulent flow at various degrees of turbulence complexity in a pipe bend. Different numerical models have also been employed to predict the flow statistics of turbulent flow in curved pipes. These include the Reynolds-averaged Navier–Stokes (RANS) model (Wilcox, 1994; Durbin, 2011), Reynolds stress (RS) model (Noorani, 2015; Rohrig et al., 2015), Eddy-viscosity (EV) model (Wallin and Johansson, 2002) and renormalization group (RNG) model (Hilgenstock and Ernst, 1996), k–ε model (Rahimzadeh et al., 2012), RNG k–ε model (Hellstrom and Fuchs, 2007) and k–ω model (Di Piazza and Ciofalo, 2010). Recently, with the advancement in numerical algorithms, many researchers have extensively applied Computational fluid dynamics (CFD) as a numerical tool for investigating turbulent flow in curved pipes. Crawford et al. (2007) carried out CFD modeling on a series of pipe bends with different curvature ratios of 1.3, 5, and 20 employing the standard k–ε model, realizable k–ε model, k–ω model and a Reynolds stress model (RSM). It was established that RSM yielded the most accurate pressure loss data, followed by the realizable k–ε model, then the standard k–ε model, and finally the k–ω model in that order. The turbulent viscosity coefficient for single-phase flow in pipe bends using turbulence kinetic energy and dissipation ratio are studied in Refs. (Rahimzadeh et al., 2012; Homicz, 2004; Kim et al., 2014). Röhrig et al. (2015) conducted a comparative assessment of the different computational approaches for modeling turbulent flow through a 90° pipe bend, using both RANS and LES CFD models. Dutta et al. (2016) analyzed the static pressure distribution of single-phase turbulent flow at a symmetry plane of pipe bends using the k–ε turbulence model. The performance of the different numerical models varies with the discretization

*Corresponding author: R.K. Apalowo, rkapalowo@usm.my

scheme applied. Hence, a parametric study of the sensitivity of the flow mechanism to various discretization schemes is required to overcome this limitation.

Experimental techniques and measurements have been designed to investigate turbulent flow in curved pipes. The experimental methods mainly include the Laser-Doppler (LDV) measurement (Al-Rafai et al., 1990; Enayet et al., 1982), hot-wire anemometry (Azzola et al., 1986; Lee et al., 2007) and Pitot tube measurement (Rowe, 1970). Al-Rafai et al. (1990) performed a Laser-Doppler (LDV) measurement of turbulent flow in 90° pipe bends and determined the influence of the bend curvature on the flow statistics. It was established that secondary flows are stronger in pipes with smaller bends. Enayet et al. (1982) also conducted LDV measurement of turbulent flow in a 90° pipe bend. The mean streamwise velocity, turbulence intensity, and static pressure of the turbulent flow were measured at different cross-stream angles. LDV measurements for turbulent flow in a U-bend pipe were performed by Azzola et al. (1986). The turbulent flow's RMS and azimuthal velocity components were computed downstream of the bend. The contribution of Azzola et al. was extended by Lee et al. (2007) to perform flow statistic measurements at different cross-stream angles in a 180° bend using hot-wire anemometry. Similarly, Anwer et al. (1989) and Anwer and So (1990) performed hot-wire anemometry measurements for turbulent flow in a U-bend. Turbulence statistics were measured at different angles up and downstream of the bend. Investigations of turbulent flows in 90° and 180° pipe bends were performed by Sudo et al. (1998; 2000) using the rotating hot-wire anemometry measurements. The turbulent statistics of the flow, such as the RMS and mean streamwise velocities, were computed.

Many researchers have contributed to a large body of theoretical, experimental, and numerical works on turbulent flows in curved portions of pipes; however, only a small number of these works discuss the impact of high Reynolds number flow and bend curvature ratio on turbulent statistics for 90-degree pipe bends (Dutta et al., 2022; Ayala and Cimbala, 2021; Jurga et al., 2022). Studies on the investigation of turbulence flow parameters, such as the mean streamwise and root mean square velocities, static pressure, and turbulent viscosity at different cross-stream angles around a 90° pipe bend, have majorly been experimental. Considering the cost implication, among other factors, of setting up a fluid dynamics experimental rig and with the recent advancement in computational fluid dynamics technology providing efficient and cost-effective numerical solutions, such as the ANSYS FLUENT, implementing a CFD numerical tool to investigate the turbulence flow parameters will complement and extend the current literature. Compared to the experimental approach, the CFD methodology is cost-effective, efficient, and easy to set up.

The main contribution of this paper includes the simulation of turbulent flow in a 90° pipe bend and the computation of the mean streamwise and RMS velocities, static pressure, and turbulent viscosity of the flow at different cross-stream angles around the bend, using numerical methods based on CFD, to investigate the influence of bend curvature on the flow parameters.

2. Methodology

2.1. Description of the Study Case

The problem considered in this study is the turbulent fluid flow through a circular-sectioned 90° bend pipe having a uniform diameter through its channel with an inside diameter (D_1) of 43 mm. By taking advantage of the symmetric geometry of the pipe, only a half-round size of the pipe is modeled.

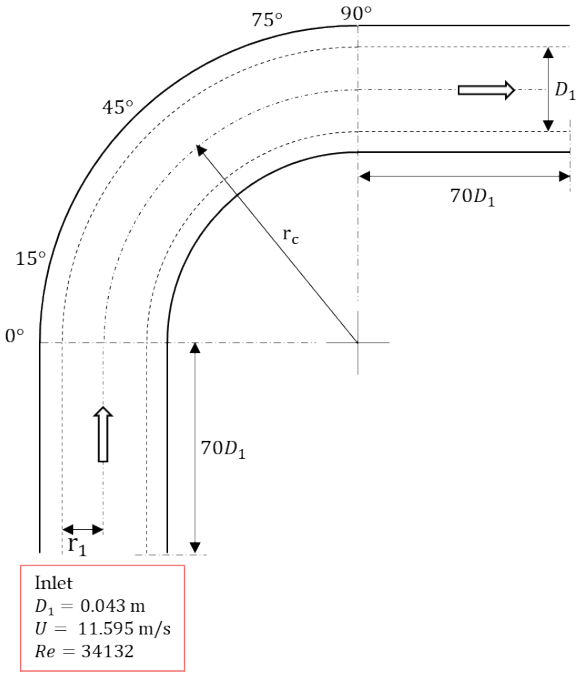

Figure. 1: Configuration of the investigated 90° pipe bend.

From the inlet, a straight upstream channel of length $70D_1$ precedes the test bend to aid proper flow development before the fluid enters the bend, which is of $7D_1$ radius of curvature. The curvature ratio *C.R.* of the pipe bend

$$C.R. = \frac{r_1}{r_c} \tag{1}$$

is computed as 1:13.95. A similar straight downstream channel of length $70D_1$ supersedes the test bend. For the turbulent flow, air is introduced into the pipe at a bulk velocity of 11.616 m/s and a Reynolds number of 34132.

The dimensions and geometry of the pipe bend (Figure 1) are similar to the ones used in the Doppler anemometry experimental measurement conducted by Al-Rafai et al. (1990). The experimental results are used to validate the numerical predictions obtained in this study.

Flow measurements at different cross-stream planes along the full length of the bend are considered. This is to study the bend curvature regions on the hydraulic performance phenomena, namely velocity distribution, static pressure, and turbulent viscosity. The performance phenomena are measured at 0° (entry), 15°, 30°, 45°, 60°, 75° and 90° cross-stream planes along the bend. All modeling and analyses are conducted in ANSYS FLUENT 19.2.

2.2. Governing equations of turbulent flow

The governing equation of the turbulent flow is based on the Reynolds-Averaged Navier-Stokes (RANS) equation. The three-dimensional RANS equations are computed from the instantaneous Navier–Stokes equations, which separate the flow variables into the mean and the fluctuating components. The equations are numerically solved using the finite volume method.

The governing equations for incompressible flow, which are based on the fundamental conservation laws of mass and momentum, can be expressed as

$$\frac{\partial}{\partial x_i}u_i = 0$$
$$\rho\frac{\partial}{\partial t}u_i + \rho\frac{\partial}{\partial x_j}u_i u_j = -\frac{\partial P}{\partial x_i} + \mu\frac{\partial^2}{\partial x_j^2}u_i - \rho\frac{\partial}{\partial x_j}\,\tau \qquad (2)$$

where u is the mean velocity, ρ the fluid density, P the mean pressure, μ the kinematic viscosity, τ the specific Reynolds stress tensor.

A preliminary study was conducted for different turbulence models to determine the accuracies of the different models in solving the problem. Based on the outcome of the preliminary study and due to its robust formulation, wide documentation reliability and affordability, lower computational overhead, and excellent performance for many industrially relevant flows, the k–ε turbulence model is applied for the analyses conducted in this study. The governing transport equations for k–ε model have the turbulent kinetic energy k expressed as

$$\frac{\partial}{\partial t}(\rho k) + \frac{\partial}{\partial x_i}(\rho k u_i) =$$
$$= \frac{\partial}{\partial x_j}\left[\left(\mu + \frac{\mu_t}{\sigma_k}\right)\frac{\partial k}{\partial x_j}\right] + P_k + P_b - \rho\varepsilon - Y_M + S_k \qquad (3)$$

with the dissipation ε expressed as

$$\frac{\partial}{\partial t}(\rho\varepsilon) + \frac{\partial}{\partial x_i}(\rho\varepsilon u_i) = \frac{\partial}{\partial x_j}\left[\left(\mu + \frac{\mu_t}{\sigma_\varepsilon}\right)\frac{\partial \varepsilon}{\partial x_j}\right] +$$
$$+ C_{1\varepsilon}\frac{\varepsilon}{k}(P_k + C_{3\varepsilon}P_b) - C_{2\varepsilon}\rho\frac{\epsilon^2}{k} + S_\varepsilon \qquad (4)$$

and the turbulent viscosity is expressed as

$$\mu_t = \rho C_\mu \frac{k^2}{\varepsilon} \qquad (5)$$

where P, Y and S are components of the deformation rate. Based on extensive examination of a wide range of turbulent flows, the constant parameters used in the equations are C_μ=0.09, σ_k=1.00, σ_ε=1.30, $C_{1\varepsilon}$=1.44 and $C_{2\varepsilon}$=1.92.

2.3. Materials and boundary conditions

The materials used for the fluid and the solid pipe in this study are air and aluminum, respectively. Conducting CFD analysis on the test bend requires describing boundary conditions for each boundary surface. The modeled pipe has four boundary surfaces: the inlet, outlet, wall, and symmetry.

The inlet boundary condition is the velocity inlet, which was evaluated from the Reynolds number Re and other parameters of the pipe as follows:

$$U = \frac{\mu Re}{\rho D} \qquad (6)$$

where μ and ρ are the fluid viscosity and density, and D is the pipe diameter. The inlet velocity was computed as 11.595 m/s. Turbulence specification method of intensity and hydraulic diameter was applied at the inlet. Turbulent intensity of 5% was used, and the hydraulic diameter D_h was calculated as 10.75 m using the relation:

$$D_h = \frac{4A}{P_w} \qquad (7)$$

where A and P_w are the cross-sectional area and wetted perimeter of the pipe.

The outlet boundary condition is the pressure outlet with turbulence specifications, intensity, and hydraulic diameter similar to the velocity inlet. A stationary boundary condition is applied at the wall boundary surface, with a roughness of 0 m, a roughness constant of 0.5, and a no-slip shear condition for the velocity. The symmetry boundary condition is applied at the symmetry surface since half of the pipe geometry is being modeled.

2.4. Mesh Generation and Grid Independence Analysis

ANSYS Design-Modeller is used to create the pipe geometry, and by taking advantage of its symmetric geometry, only a half section of the pipe is modeled to save computational cost. 3D structured hexahedral elements are used, and the mesh is generated in ANSYS ICEM. In creating the mesh, high-resolution grid divisions are adapted for the bend and the regions near the wall to ensure the accuracy of the flow parameters (such as velocity and pressure), which rapidly change around these regions. The wall y^+ is plotted to verify the mesh spacing, and it ranged from $3 < y^+ < 9$. Consequently, since the standard wall function is applicable for $y^+ > 30$, then the enhanced wall treatment is preferred.

The quality of the mesh greatly influences the accuracy of the numerical simulation. A very fine mesh is computationally more efficient but expensive. On the other hand, there is a great need to eliminate the dependence of the calculation results on the grid size to ensure the results' accuracy. Therefore, a trade-off needs to be established for the accuracy of the results, the mesh grid size, and the independence of the results on the grid size needs to be established. A convergence test was conducted for mesh grid independence by using different mesh size schemes. Table 1 presents the results obtained by comparing the velocity magnitude calculated through each meshing scheme against the experimental results obtained through Laser Doppler measurement in Al-Rafai et al. (1990).

As presented in Table 1, it can be observed that the result accuracy increases as the mesh size reduces. Convergence was observed between the meshing schemes 4 and 6, in which their % deviations differ by just 0.02. Reducing the mesh size further would only increase

the computational time without significantly improving the result accuracy. Therefore, the meshing scheme 4 was adopted for the calculations in this study.

Table 1: Mesh grid size convergence analysis based on the flow velocity magnitude.

Mesh Scheme	No. of Elements	No. of Nodes	Velocity magnitude (m/s)	% Deviation*
1	10177	43,761	13.284	6.61
2	28353	116530	13.396	5.82
3	71337	289628	13.642	4.09
4	111500	452690	13.760	3.26
5	218941	888903	13.761	3.25
6	286308	1081213	13.763	3.24

*Experimental measurement as reference

2.5. Solution scheme and convergence

The numerical computations conducted in this study applied the SIMPLE algorithm, which is based on finite volume discretization. Different discretization schemes, such as the first-order upwind, second-order upwind, and QUICK, are used to analyze all flow situations. The different schemes were used to achieve a range of accuracy and provide a basis for comparisons.

Upon setting the solution criteria, a convergence criterion of 0.0001 was applied to converge the residuals. The number of iterations for the calculation was set at 300 since the solution will converge at the residual's condition, and iterations will stop when those criteria are met, as shown in Figure 2.

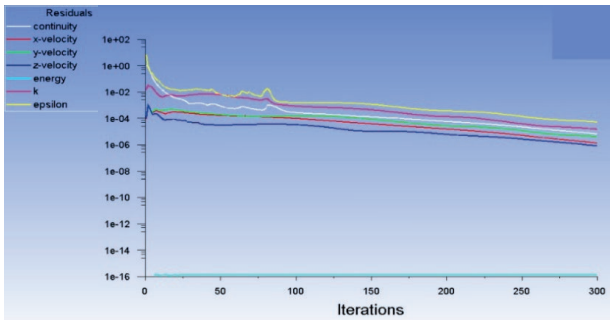

Figure 2: Convergence plot of the simulation residuals.

3. Numerical results and discussion

3.1. Flow development

The airflow travels $70D_1$ upstream through the pipe before entering the bend. Figure 3 presents the flow physics around the bend region, suggesting a secondary flow due to fluid acceleration and deceleration due to the pipe bend curvature. The outer wall region shows a high velocity and shear stress resulting from the impact of the fluid due to the change in the direction of the fluid motion in an erratic fashion. A velocity magnitude of 13.76 m/s is noticed at the outer wall region throughout the pipe bend.

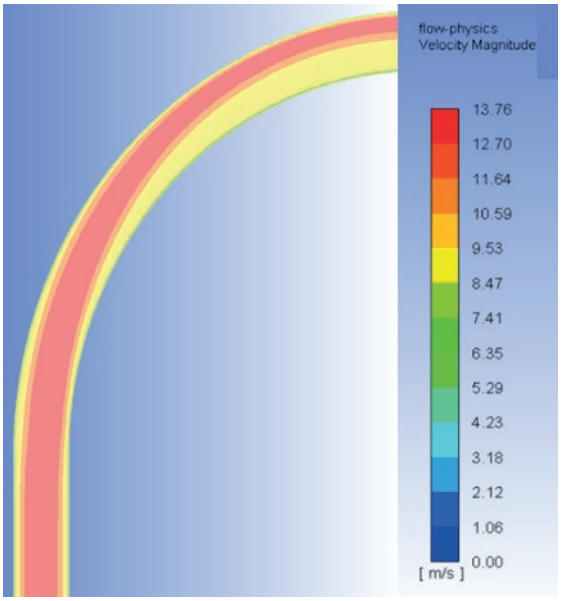

Figure 3: Flow physics velocity magnitude at the bend entry.

The velocity profile of the flow development at the bend entry is presented in Figure 4. This profile shows that the flow has fully developed at the bend entry.

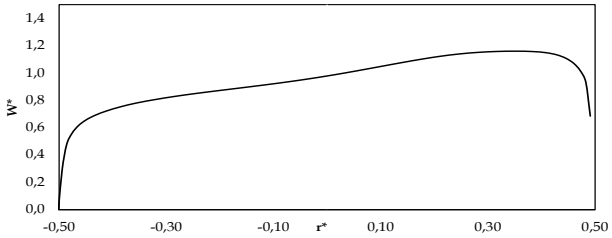

Figure 4: Streamwise velocity profile of the flow development at the bend entry.

3.2. Comparative analysis of different turbulence models

Preliminary analysis was conducted to investigate the capability of the different turbulence models for modeling the turbulent flow along the bend. The models investigated include k–ε, k–ω, Spalart-Allmaras, Transition-SST, and Reynold stress turbulence models. These were investigated using different spatial discretization schemes. The normalized mean streamwise velocity is computed along the plane of symmetry at 45° for the different turbulence models to investigate each model's accuracy. The results of the streamwise velocity are normalized (W*) by the fluid bulk velocity of 11.595 m/s. The accuracy of each model is evaluated using the standard percentage error, computed as

$$\% \text{ Error} = \frac{\sum_{k=1}^{N} |W_{N,k}^{*} - W_{E,k}^{*}|}{\sum_{k=1}^{N} W_{E,k}^{*}} \times 100 \quad (8)$$

where $W^*_{N,k}$ and $W^*_{E,k}$ are respectively the numerical and experimental normalized mean streamwise velocities along the nodal points of the symmetry plane. N is the number of nodal points. The results obtained from the preliminary analysis is summarised as presented in Table 2.

Table 2: Summary of the turbulence models error analysis.

	Discretization Schemes		
	FOU	2OU	QUICK
Turbulent Model		% Error*	
Spalart-Allmaras	3.27	3.37	3.37
Standard k–ε	4.56	3.93	4.69
RNG k–ε	-	3.97	-
Realizable k–ε	3.83	3.97	3.96
Standard k–ω	-	4.21	-
BSL k–ω	-	4.21	-
SST k–ω	-	4.22	-
Transition SST	-	4.25	-
Reynold stress	-	4.03	-

*Experimental measurement as reference; FOU – First-order upwind scheme; 2OU – Second-order upwind scheme.

The results show that the realizable k–ε and Spalart-Allmaras models exhibited the best agreements with the experimental measurements, with respective errors of 3.83% and 3.27%. The realizable k–ε is therefore adapted for all calculations in this study due to its robust formulation and excellent performance for many industrially relevant flows.

3.3. Root mean square velocity prediction

The numerical predictions of the root mean square (RMS) velocities at 0°, 15°, 45° and 90° around the bend are compared with the experimental measurements in Figures 5, 6, 7, and 8, respectively.

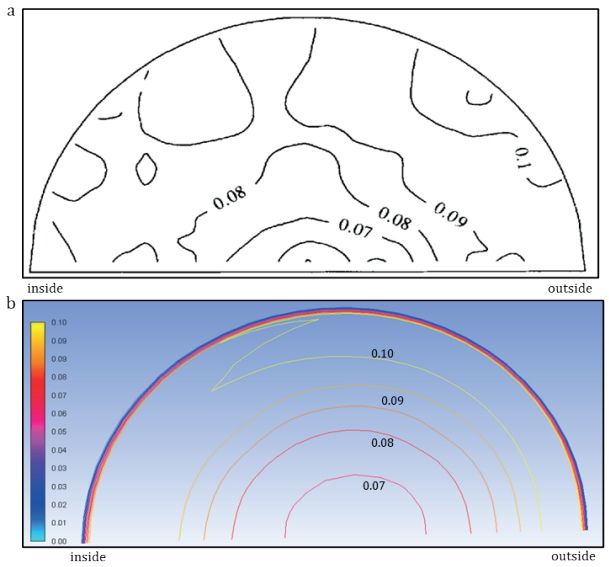

Figure 5: Experimental (a) and numerical (b) root mean square velocities at 0° (unit in m/s).

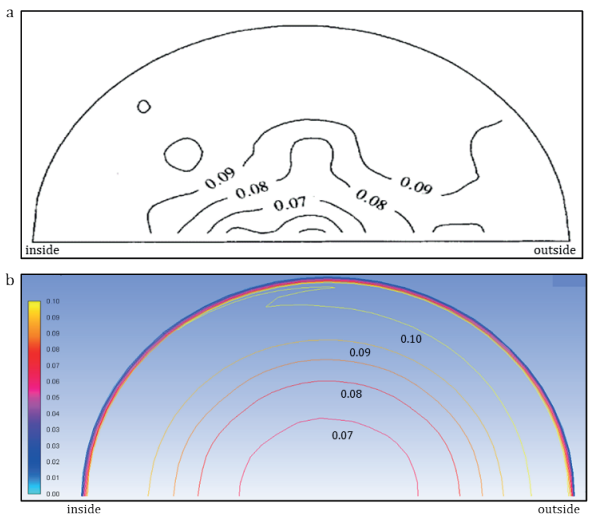

Figure 6: Experimental (a) and numerical (b) root mean square velocities at 15° (unit in m/s).

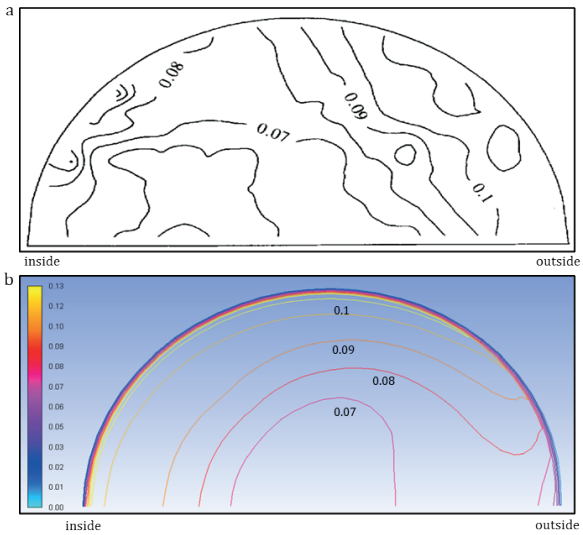

Figure 7: Experimental (a) and numerical (b) root mean square velocities at 45° (unit in m/s).

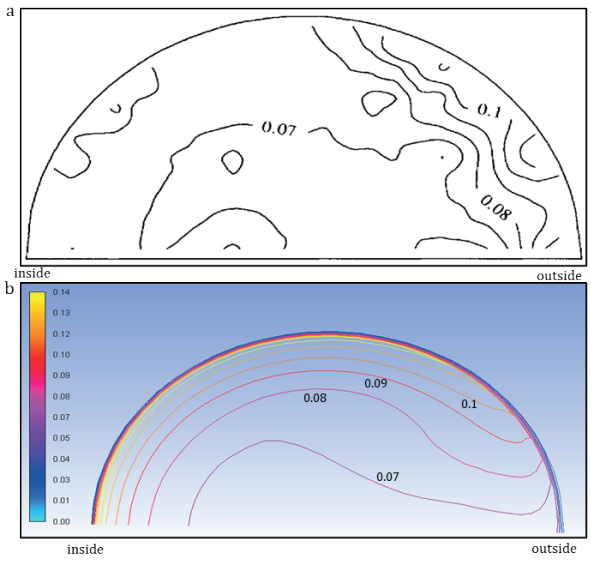

Figure 8: Experimental (a) and numerical (b) root mean square velocities at 90° (unit in m/s).

Pipe bends introduce flow structures that initiate energy loss and heat transfer, causing the flow to switch erratically due to curvature. As shown in Figures 5 and 6, it is observed that the RMS velocities at 0° and 15° are relatively low as a result of small boundary layer thickness (Al-Rafai et al., 1990). This indicates that the secondary flow developed is being created at the entry of the pipe and might be weak upon development. As shown in Figure 7, higher RMS velocities are observed at 45°, the angle where the flow seems to have a greater wall shearing and an increased turbulent viscosity and energy. The larger RMS values at 45° may be due to the increase in the circulation of the

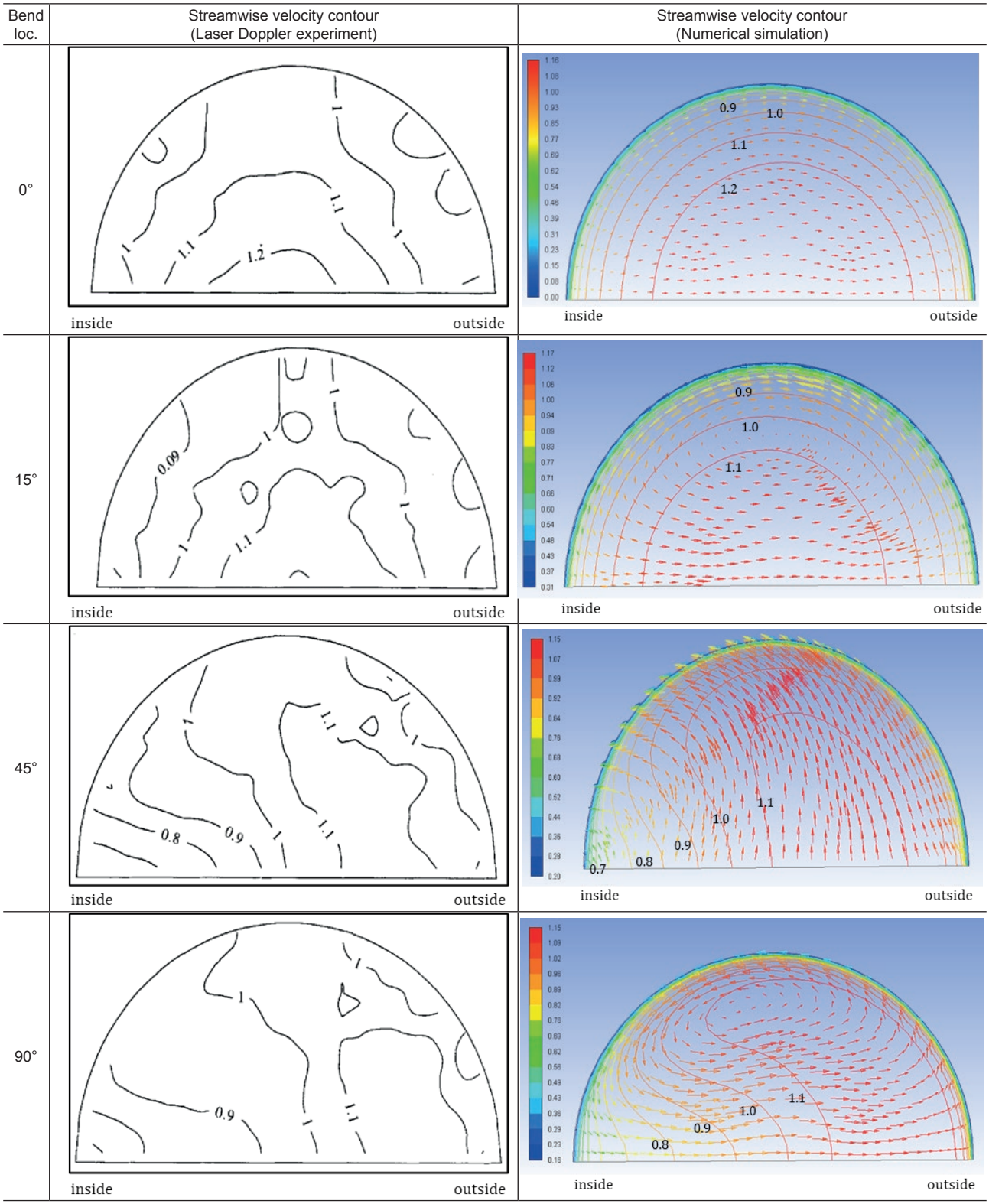

Figure 9: Comparison of the experimental and numerically computed streamwise velocities at different locations around the bend (unit in m/s).

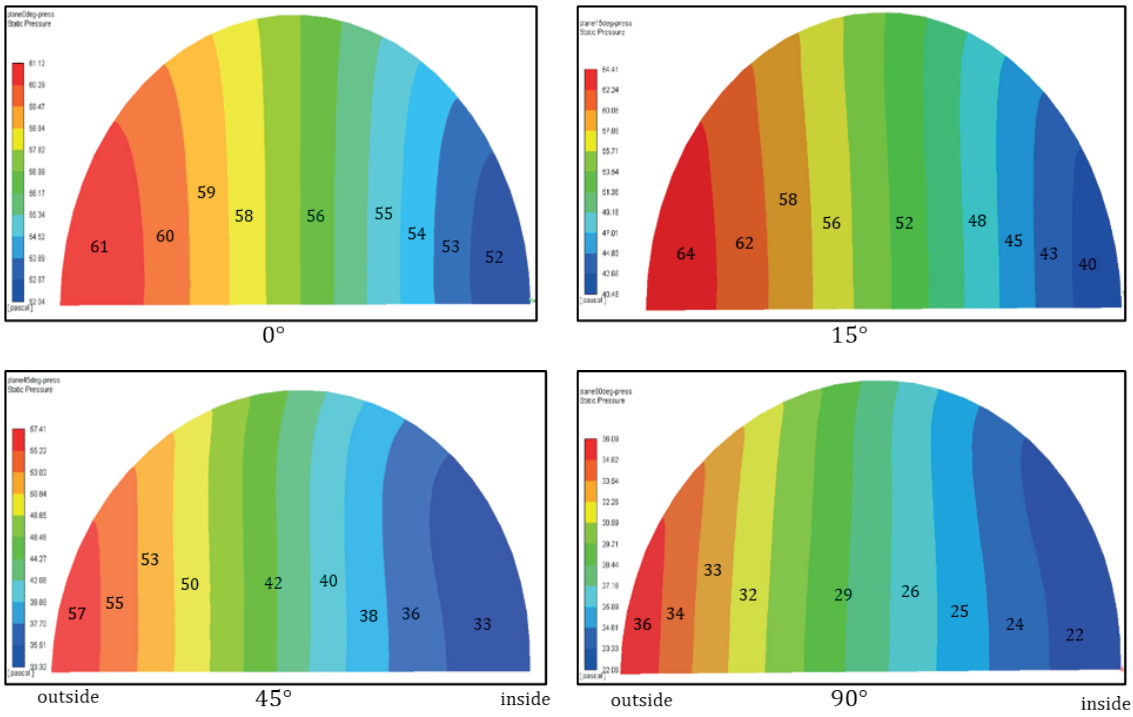

Figure 10: Predicted static pressure of the flow at different locations around the bend (unit in Pa).

Dean vortices, indicating a turbulent generation. Also, at this angle, the flow generally tends towards the outer region of the pipe bend. However, at 90°, the high-velocity fluid shifts towards the inner wall region, as shown in Figure 8. Generally, the RMS velocity continues to increase substantially along the pipe bend, as depicted in Figures 5-8. The numerical predictions satisfactorily agree with the experimental data, as shown in Figures 5-8.

3.4. Streamwise velocity prediction

The numerical results of the streamwise velocity predictions at 0°, 15°, 45° and 90° around the bend are compared with the experimental measurements, as presented in Figure 9. At the bend entry -0°, the secondary flow motion is still weak; however, at 15°, strong secondary flow is developed as the fluid flows upstream of the pipe bend. Though no serious pressure effect is observed at this stage, the fluid vortex is being created because of the impact of bend curvature. At 45°, it is observed that there is a swirling motion of the fluid with a counter-rotating fluid flow inside the pipe bend. This can be the effect of the imbalances between the pressure gradients and centrifugal forces produced by the air blower. The adverse effect of the pressure fluctuations is seen at 45°, especially at the outer wall, and favorable at the inner wall.

Comparing the streamwise velocity contour plots of the CFD numerical simulation and the experimental measurements, it is observed that there is a substantial level of agreement in the results. This validates the ANSYS CFD-Fluent as a reliable tool for conducting computational fluid dynamics and analyzing the fluid flow behavior around pipe bends.

3.5. Static pressure prediction

The numerical predictions of the flow static pressure at 0°, 15°, 45° and 90° around the bend are presented in the pressure contours shown in Figure 10. It is observed that the static pressure is higher at the outer region of the wall. The higher-pressure region at the outer wall is due to flow deceleration or swirling due to the bend (Chowdhury et al., 2016). The streamwise velocity can be influenced by the streamwise pressure gradient, which has an adverse effect near the outside of the bend.

The static pressure of the flow along the plane of symmetry at 0°, 45° and 75° are shown in Figure 11. Pressure distributions due to the bend radius along the pipe are observed, propagating secondary flow. Pressure build-up reaches the maximum when the flow reaches the region of 45° along the plane of symmetry. The turbulent kinetic energy, which results from the propagated secondary

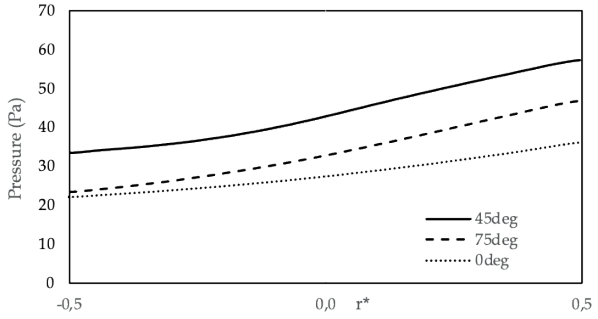

Figure 11: Static pressure of the flow at different locations.

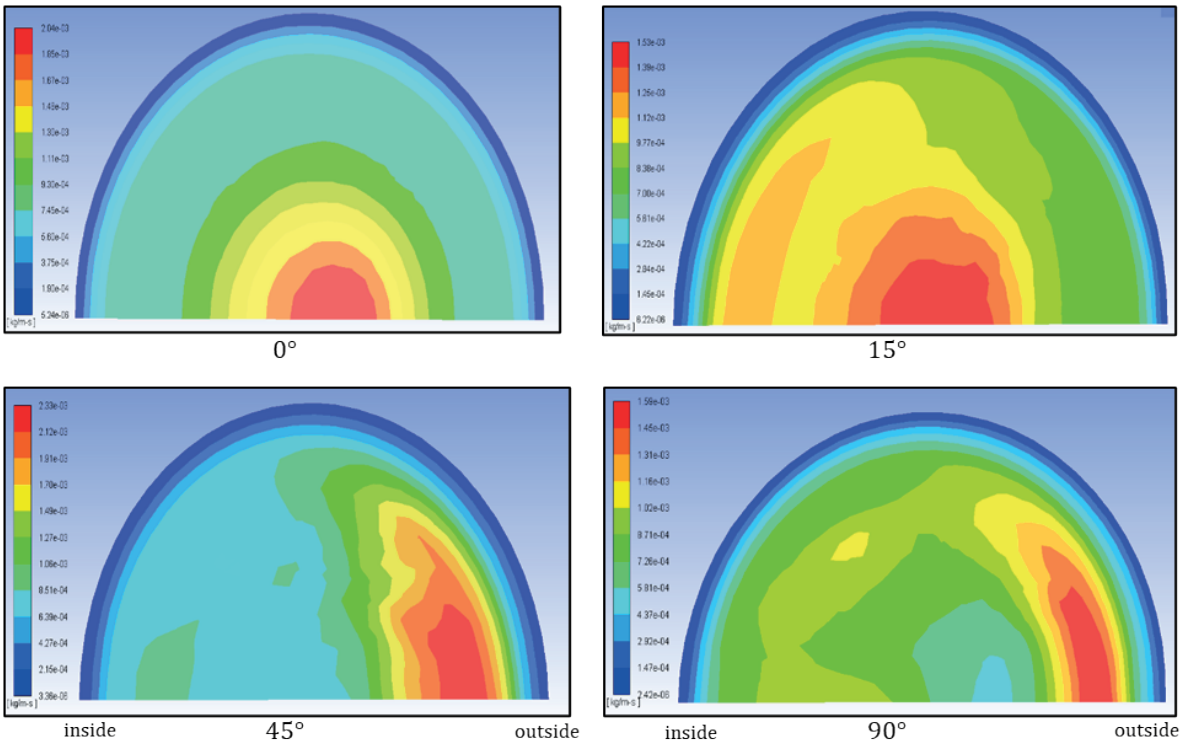

Figure 12. Predicted turbulent viscosity of the flow at different locations around the bend (unit in kg/m-s)

flow effect, reaches the maximum at the walls of the pipe bend. The high magnitude of the kinetic energy at the wall region results from the extra strain rate imposed by the curvature, indicating flow impingement on the outer wall down the bend. Consequently, recovery from the effect of bend curvature may take a longer distance down the pipe, suggesting turbulence-induced erosion of the pipe wall.

3.6. Turbulent viscosity prediction

The numerical predictions of the flow turbulent viscosity at 0°, 15°, 45° and 90° around the bend are presented in Figure 12.

The flow turbulent viscosity has much stability at 0°. This is understandable since the secondary flow has not been developed yet, and the boundary layer thickness is still small. As the fluid travels further, there is an emergence of flow separation and an increase in the turbulent viscosity at 15°. This can lead to perturbation and turbulence-induced vibrations from the effect of bend curvature. This flow separation seems to be predominant on the inside of the bend. As the flow progresses, the turbulent viscosity at the wall becomes higher at 45° with high RMS velocity values. This is due to an increase in the circulation of the Dean vortices, an indication of the emergence of turbulence, which continues up to 90° around the bend. Meanwhile, the flow-accelerated corrosion, which mainly results from the high shear stress side of the flow field (Chowdhury et al., 2016), becomes more evident at 45°.

The turbulent viscosity of the flow along the plane of symmetry at 0°, 45° and 75° are shown in Figure 13. It is observed that the viscosity is high at the outer region of the wall and suppressed at the inner region of the wall,

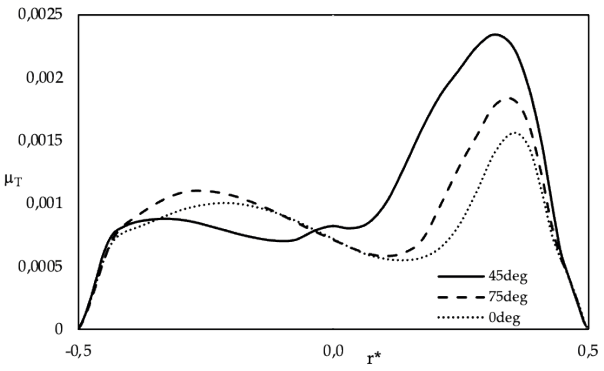

Figure 13. Turbulent viscosity of the flow at different locations along the symmetry (unit in kg/m-s).

implying that curvature affects the flow field stability. As shown in Figure 13, a further reduction in the bend radius will lead to an increase in the turbulent viscosity, which will adversely affect the flow structure and energy, as well as difficulty in damping the viscosity.

4. Conclusions

The main objective of this study was to investigate the behavior of turbulent flow parameters around the bend curvature of a curved pipe using numerical computational fluid dynamics (CFD) simulations. The study investigated the behavior of turbulent flow parameters, such as the root mean square (RMS) and streamwise velocities, static pressure, and turbulent intensity, around the bend

curvature of a 90° curved pipe using the numerical computational fluid dynamics tool, ANSYS Fluent. The pipe bend has a curvature ratio of 1:13.95. For the turbulent flow, air is introduced into the pipe at a bulk velocity of 11.616 m/s and a Reynolds number of 34 132. Flow behaviors were studied at different cross-stream planar angles of the bend and different angles along the plane of symmetry. The numerical predictions were compared against available experimental measurements. The main conclusions reached are as follows:

(i) Good agreements are observed between the numerical predictions and the available experimental measurements, with a maximum disparity of 3.83%.

(ii) The high intensity of secondary flow and turbulence energy, driven towards the outside of the pipe bend, is the effect of imbalances in the pressure distributions along a pipe bend, with the most adverse impact recorded at about 45°.

(iii) The RMS velocity is observed to be larger near the wall, especially at the outer wall region. Also, the RMS velocity is highest at 45° along the bend due to increased circulation of Dean vortices, indicating a turbulence generation. The RMS velocity increases downstream along the pipe bend due to an additional mean strain resulting from the creation of secondary flow as the flow travels through the bend.

(iv) The maximum pressure and turbulent viscosity are recorded at the outer wall of the pipe bend due to flow deceleration and swirling along the outer wall. However, the turbulent viscosity is suppressed near the inner wall. Thus, it can be established that the bend curvature influences the stability of the flow field inside the pipe bend.

The above concluding remarks refer to the current study scope. Extending the scope to loss coefficients, the secondary vortex intensity, and the turbulent parameters for different curvature ratios will be the focus of future research.

References

Apalowo, R.K. (2022). Numerical study of different models for turbulent flow in 90° pipe bend, *University of Porto Journal of Engineering, 8*(2), 121-134. https://doi.org/10.24840/2183-6493_008.002_0010

Al-Rafai, W.N., Tridimas, Y.D., Woolley, N.H. (1990). A Study of Turbulent Flows in Pipe Bends, *Proceedings of the Institution of Mechanical Engineers, Part C, 204*(6), 399-408. https://doi.org/10.1243/PIME_PROC_1990_204_120_02

Anwer, M., So, R.M.C., Lai, Y.G. (1989). Perturbation by and Recovery from Bend Curvature of a Fully Developed Turbulent Pipe Flow, *Physics of Fluids, 1*(8), 1387, 1989. https://doi.org/10.1063/1.857315

Anwer, M., So, R.M.C. (1990). Frequency of Sublayer Bursting in a Curved Bend. *Journal of Fluid Mechanics, 210*, 415-435. https://doi.org/10.1017/S0022112090001343

Ayala, M., Cimbala, J.M. (2021). Numerical approach for prediction of turbulent flow resistance coefficient of 90 pipe bends, *Proceedings of the Institution of Mechanical Engineers, Part E: Journal of Process Mechanical Engineering, 235*(2), 351-360. https://doi.org/10.1177/0954408920964008

Azzola, J., Humprey, J.A.C., Iacovides, H., Launder, B.E. (1986). Developing Turbulent Flow in a U-Bend of Circular Cross-Section: Measurement and Computation, *ASME Journal of Fluids Engineering, 108*(2), 214-221. https://doi.org/10.1115/1.3242565

Boersma, B.J., Nieuwstadt, F.T.M. (1996). Large-Eddy simulation of turbulent flow in a curved pipe, *Journal of Fluids Engineering, 118*(2), 248-254. https://doi.org/10.1115/1.2817370

Chowdhury, R.R., Biswas, S., Alam, M.M., Islam, A.S. (2016). Turbulent flow analysis on bend and downstream of the bend for different curvature ratio, In *AIP Conference Proceedings, 1754*(1), 040020. https://doi.org/10.1063/1.4958380

Crawford, N.M., Cunningham, G., Spence, S.W.T. (2007). An experimental investigation into the pressure drop for turbulent flow in 90 elbow bends. *Proceedings of the Institution of Mechanical Engineers, Part E: Journal of Process Mechanical Engineering, 221*(2), 77-88. https://doi.org/10.1243/0954408JPME84

Di Piazza, I., Ciofalo, M. (2010). Numerical Prediction of Turbulent Flow and Heat Transfer in Helically Coiled Pipes, International. *Journal of Thermal Science, 49*(4), 653-663. https://doi.org/10.1016/j.ijthermalsci.2009.10.001

Durbin, P A., Pettersson-Reif, B.A. (2011). *Statistical Theory and Modelling for Turbulent Flows*, 2nd ed. Wiley, Chichester, UK. https://doi.org/10.1002/9780470972076

Dutta, P., Saha, S.K., Nandi, N., Pal, N. (2016). Numerical study on flow separation in 90 degree pipe bend under high Reynolds number by modelling, *Engineering Science and Technology, 19*, 904-910. https://doi.org/10.1016/j.jestch.2015.12.005

Dutta, P., Chattopadhyay, H., Nandi, N. (2022). Numerical studies on turbulent flow field in a 90 deg pipe bend, *Journal of Fluids Engineering, 144*(6), 061104. https://doi.org/10.1115/1.4053547

Enayet, M.M., Gibson, M.M., Taylor, A., Yianneskis, M. (1982). Laser-Doppler Measurements of Laminar and Turbulent Flow in a Pipe Bend, *International Journal of Heat Fluid Flow, 3*(4), 213-219. https://doi.org/10.1016/0142-727X(82)90024-8

Hellstrom, F., Fuchs, L. (2007). Numerical Computations of Steady and Unsteady Flow in Bended Pipes, *AIAA Paper*, No. 2007-4350. https://doi.org/10.2514/6.2007-4350

Hilgenstock, A., Ernst, R. (1996). Analysis of Installation Effects by Means of Computational Fluid Dynamics-CFD versus Experiments, *Flow Measurement and Instrumentation, 7*(3-4), 161-171. https://doi.org/10.1016/S0955-5986(97)88066-1

Homicz, G.F. (2004). *Computational Fluid Dynamic Simulations of Pipe Elbow Flow*. United States, Department of Energy. https://doi.org/10.2172/919140

Jurga, A.P., Janocha, M.J., Yin, G., Ong, M.C. (2022). Numerical simulations of turbulent flow through a 90-deg pipe bend, *Journal of Offshore Mechanics and Arctic Engineering, 144*(6), 061801. https://doi.org/10.1115/1.4054960

Kim, J., Yadav, M., Kim, S. (2014). Characteristics of secondary flow induced by 90-degree elbow in turbulent pipe flow, *Engineering Applications of Computational Fluid Mechanics, 8*(2), 229-239. https://doi.org/10.1080/19942060.2014.11015509

Lee, G.H., Choi, Y.D., Han, S.H. (2007). Measurement of Developing Turbulent Flow in a U-Bend of Circular Cross-Section, *Journal of Mechanical Science and Technology, 21*(2), 348-359. https://doi.org/10.1007/BF02916295

Noorani, A. (2015). *Particle-Laden Turbulent Wall-Bounded Flows in Moderately Complex Geometries*, Ph.D. thesis, KTH Mechanics, Stockholm, Sweden.

Rahimzadeh, H., Maghsoodi, R., Sarkardeh, H., Tavakkol, S. (2012). Simulating flow over circular spillways by using different turbulence models, *Engineering Applications of Computational Fluid Mechanics, 6*(1), 100-109. https://doi.org/10.1080/19942060.2012.11015406

Rohrig, R., Jakirlic, S., Tropea, C. (2015). Comparative Computational Study of Turbulent Flow in a 90 Degree Pipe Elbow, *International Journal of Heat Fluid Flow, 55*(ETMM10), 102-111. https://doi.org/10.1016/j.ijheatfluidflow.2015.07.011

Rowe, M. (1970). Measurements and Computations of Flow in Pipe Bends, *Journal of Fluid Mechanics, 43*(4), 771-783. https://doi.org/10.1017/S0022112070002732

Schiestel, R. (2010). *Modelling and simulation of turbulent flows*, John Wiley & Sons.

Spedding, P.L., Benard, E., McNally, G.M. (2004). Fluid flow through 90 degree bends, *Developments in Chemical Engineering and Mineral Processing, 12*(1-2), 107-128. https://doi.org/10.1002/apj.5500120109

Sudo, K., Sumida, M., Hibara, H. (1998). Experimental Investigation on Turbulent Flow in a Circular-Sectioned 90-Degree Bend, *Experiment in Fluids, 25*(1), 42-49. https://doi.org/10.1007/s003480050206

Sudo, K., Sumida, M., Hibara, H. (2000). Experimental Investigation on Turbulent Flow through a Circular-Sectioned 180-Degree Bend, *Experiment in Fluids, 28*(1), 51-57. https://doi.org/10.1007/s003480050007

Wallin, S., Johansson, A.V. (2002). Modelling Streamline Curvature Effects in Explicit Algebraic Reynolds Stress Turbulence Models, *International Journal of Heat Fluid Flow, 23*(5), 721-730. https://doi.org/10.1016/S0142-727X(02)00168-6

Wilcox, D. C. (1994). *Turbulence Modelling for CFD*, DCW Industries, La Canada Flintridge, CA.